Research Article | Vol. 28, No. 26 / 21 December 2020 / Optics Express 38907
Optics EXPRESS

Refractive index sensing with optical bound states in the continuum

DMITRII N. MAKSIMOV,[1,2,*] VALERIY S. GERASIMOV,[1,3] SILVIA ROMANO,[4] AND SERGEY P. POLYUTOV[1]

[1]Siberian Federal University, 660041, Krasnoyarsk, Russia
[2]Kirensky Institute of Physics, Federal Research Center KSC SB RAS, 660036, Krasnoyarsk, Russia
[3]Institute of Computational Modeling SB RAS, Krasnoyarsk, 660036, Russia
[4]Institute of Applied Sciences and Intelligent Systems, National Research Council, Naples, 80131, Italy
*mdn@tnp.krasn.ru

Abstract: We consider refractive index sensing with optical bounds states in the continuum (BICs) in dielectric gratings. Applying a perturbative approach we derived the differential sensitivity and the figure of merit of a sensor operating in the spectral vicinity of a BIC. Optimisation design approach for engineering an effective sensor is proposed. An analytic formula for the maximal sensitivity with an optical BIC is derived. The results are supplied with straightforward numerical simulations.

1. Introduction

Bound states in the continuum (BICs) have revolutionized nanophotonics offering the opportunity to realize a new class of high throughput sensing devices and improving the control of the interaction between light and matter at the nanometer scale [1–10]. Strictly speaking, a BIC can be considered as a resonant mode with an infinite quality factor (Q-factor) in an open cavity. A BIC has a frequency in the radiation continuum but does not lose energy because of symmetry mismatch with outgoing waves. The BICs are hosted by a leaky band of high-quality resonances with Q-factor diverging in the Γ-point [11]. The leaky band with diverging Q-factor, in turn, induces a collapsing Fano feature in the transmittance spectrum [12–15]. Generally, the position of these extremely narrow Fano resonances is sensitive to the refractive index of the surrounding medium allowing to engineer optical sensors with a good sensitivity, S and an excellent figure of merit (FOM) [16]. The sensitivity is affected by the spatial overlap between the nonradiating evanescent field and the surrounding cladding, while FOM is proportional to the Q-factor and ultimately represents the sensor capability to follow tiny changes in the environment refractive index [17,18]. Among the different geometries of structures supporting BICs, all-dielectric resonant planar structures, including photonic crystal slabs, periodic arrays and metasurfaces, have been taken as an alternative to conventional plasmonic sensors due to the possibility to realize high-performance sensing systems in loss-free media [16,19–23].

The major drawback of the dielectric sensors in comparison with the plasmonic ones is considerably (approximately five times) less sensitivity [24]. Therefore, it is of key importance to understand how the sensitivity can be enhanced while keeping high values of the FOM. In this paper we derive analytical expressions for S and FOM for sensors based on dielectric grating (DGs). The subwavelength DGs have recently emerged as one of the major set-ups for studying optical BICs both theoretically [25–31] and experimentally [32,33]. By using a perturbative approach we find the differential sensitivity and the figure of merit of a DG-sensor operating in the spectral vicinity of a BIC. The reported analytic results could pave a way for an optimisation design approach for engineering an effective BIC sensor, in terms of both sensitivity and FOM, and provide a tool for a better understanding of the physics underlying the mechanism of sensing.

#411749 https://doi.org/10.1364/OE.411749
Journal © 2020 Received 7 Oct 2020; revised 15 Nov 2020; accepted 20 Nov 2020; published 9 Dec 2020

Optics EXPRESS

2. Bound states in the continuum

Here we consider the system shown in Fig. 1(a). It is a dielectric grating (DG) assembled of rectangular bars. The bars are periodically placed on the glass substrate with period h. We assume that the incident field is TE polarized, i.e. the electric vector is aligned with the bars as shown in Fig. 1(a). The propagation of the TE-modes is controlled by the Helmholtz equation for the x component of the electric field:

$$\left(\frac{\partial^2}{\partial y^2} + \frac{\partial^2}{\partial z^2}\right) E_x + k^2 \epsilon E_x = 0, \tag{1}$$

where k is the vacuum wavenumber, and ϵ is the dielectric function. In what follows we assume that the bars can be made of different dielectric materials such as polycrystalline silicon, Si; and titanium dioxide, TiO_2. The refractive index (RI) of the substrate $n_0 = 1.5$.

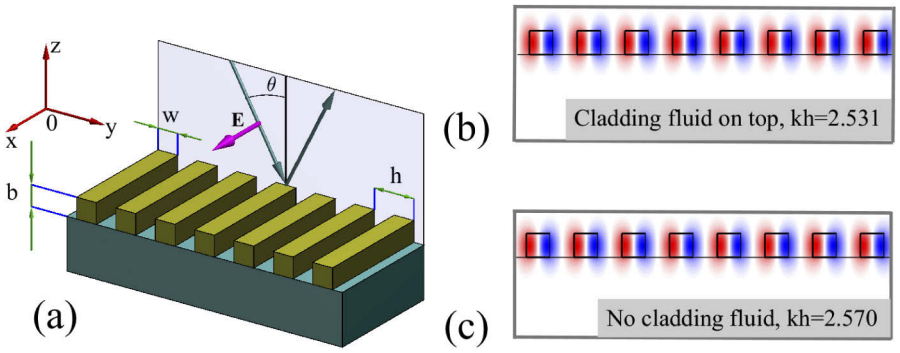

Fig. 1. (a) The dielectric grating assembled of rectangular bars on glass substrate. The plane of incidence $y0z$ is shaded grey. The magenta arrow shows the electric vector of the incident wave. The geometric parameters are $w = 0.5h$, $b = 0.5h$. (b, c) BIC eigenmode profiles for Si bars as E_y in the $y0z$-plane with ($n_c^{(0)} = 1.333$) and without ($n_c^{(0)} = 1$) cladding, correspondingly.

The RI sensor operating principle is detection of the shift in the wavelength of an optical resonance, λ_{res} in response to the change of the RI of the cladding fluid, n_c on top of the DG. As the reference value of the cladding RI we take that of water $n_c^{(0)} = 1.333$. Our finite-difference time-domain (FDTD) simulations demonstrate that for the set of geometric parameters specified in the caption to Fig. 1 a Si DG supports a BIC with $kh = 2.531$. The BIC is observed as a specific point of the leaky band dispersion with infinite life-time of the resonant mode in the Γ-point (see e.g. [15]). The field profile of the BIC in the Si DG with cladding fluid is shown in Fig. 1(b). The BIC clearly falls into the symmetry protected type as it is symmetrically mismatched to the zeroth order diffraction channel [15]. It is remarkable that the BIC mode profile is robust with respect to variations of n_c as it can be seen from Fig. 1(c), where we demonstrate the field profile of the

Table 1. BICs in dielectric gratings. The values of RI are taken at 1μm. The BIC wavelenghts, λ_{BIC} are measured in the units of *h*.

Grating material	Si	Si	TiO_2	TiO_2
Grating RI	3.575	3.575	2.485	2.485
Cladding fluid	Yes	No	Yes	No
hk	2.531	2.570	3.448	3.564
λ_{BIC}, (p.d.u.)	2.482h	2.445h	1.822h	1.761h

Optics EXPRESS

BIC at $kh = 2.570$ with no cladding fluid. Notice that the mode profiles are indistinguishable to the naked eye. This robustness of the mode profile allows for keeping the characteristics of the sensor with different cladding fluids. The simulations were also run for a DG made of Ti_20. The obtained BIC field profiles are almost identical to those in Fig. 1(b) and Fig. 1(c), and, hence, are not shown in the paper. The numerical data for both DG materials are collected in Table 1.

3. Refractive index sensing

Although the BIC proper is totally decoupled from the outgoing waves, it is spectrally surrounded by a leaky band with with a diverging Q-factor. If the DG is illuminated from the far-zone, this leaky band induces a collapsing Fano feature in the transmittance spectrum. Below we investigate into application of the collapsing Fano resonance for RI sensing. Two quantities are of major importance for engineering an effective sensor: the differential sensitivity defined as

$$S = \left.\frac{d\lambda_{\text{res}}}{dn_c}\right|_{n_c=n_c^{(0)}}, \tag{2}$$

and the figure of merit (FOM) given by

$$\text{FOM} = \frac{S}{W}, \tag{3}$$

where W is the width of the operating resonance in terms of wavelength. Here we applied the definition of the FOM used in our previous paper [16]. This definition involves two most important characteristics – the sensitivity and the linewidth of the operating resonance. The smaller linewidths are useful for increasing the limit of detection of the sensor, since only the resonance shifts larger than the linewidths are easily detectable. Thus, the larger FOM is beneficial.

Here we aim at deriving analytic expressions for both quantities of interest using a perturbative approach. The perturbative approach utilizes two small parameters: the first is the increment of the dielectric function $\Delta\epsilon_c$ due to the change of the RI of the cladding, and the second is the angle of incidence θ defined in Fig. 1(a). The solution of Eq. (1) can be written in the form of a Bloch wave due to the y-axis periodicity

$$E_x(y,z) = \psi(y,z)e^{i\beta y}, \tag{4}$$

where $\beta = k\sin(\theta)$ is the propagation constant along the y-axis. After substituting the above into Eq. (1) and taking into account $\Delta\epsilon_c$ one finds

$$\left(\frac{\partial^2}{\partial y^2} + \frac{\partial^2}{\partial z^2}\right)\psi + k^2(\mathscr{L}_c + \mathscr{L}_\theta)\psi + k^2\epsilon\psi = 0, \tag{5}$$

where the perturbation operators are given by

$$\mathscr{L}_c = \Delta\epsilon_c, \tag{6}$$

$$\mathscr{L}_\theta = 2i\frac{\sin(\theta)}{k}\frac{d}{dx} - \sin^2(\theta)\frac{d}{dx^2}. \tag{7}$$

Notice that $\mathscr{L}_c$ and $\mathscr{L}_\theta$ are independently parametrized with respect to n_c and θ. It means that the contributions of the two operators into the perturbed eigenfrequency are additive in the first perturbation order.

First let us see the effect of $\mathscr{L}_c$. In general, the application of perturbative approaches to resonant states in not trivial, since the eigenfields diverge in the far-zone [34–36]. One of the

Optics EXPRESS

possible solutions is the use of the Wigner-Brillouin (WB) perturbation theory [37,38]. The application of the WB approach requires a very specific normalization condition for the resonant states involving both "volume" convolution with dielectric function, and "flux" term as a surface integral over the outer interface of the elementary cell. It can be argued, however, that the BIC proper is a specific case when the flux term can be dropped off due to the eigenfield vanishing in the far-zone [39]. Thus, for a single BIC mode the WB perturbation theory yields vacuum wavenumber

$$k = \frac{2k^{(0)}}{2 + I_c \Delta\epsilon_c}, \tag{8}$$

where $k^{(0)}$ is the vacuum wavenumber of the BIC with the reference value of the cladding RI and

$$I_c = \int_{\mathcal{S}_c} \left(E_x^{(\mathrm{BIC})}\right)^2 dydz \tag{9}$$

with $\mathcal{S}_c$ as the area of the elementary cell occupied by the cladding fluid, and $E_x^{(\mathrm{BIC})}$ as the BIC eigenfield satisfying the following normalization condition

$$1 = \int_{\mathcal{S}} \left(E_x^{(\mathrm{BIC})}\right)^2 \epsilon(y,z) dydz, \tag{10}$$

where $\mathcal{S}$ is the total area of the elementary cell. Notice that although the integration domains are infinite both integrals converge due to the eigenfield vanishing in the far-zone.

The normalization condition (10) naturally invites applying the standard Rayleigh-Schrödinger (RS) perturbative approach following [40]. Remarkably, unlike the WB method the first order RS approach does not involve any other states rather than the unperturbed state under consideration [41]. The first order RS solution reads

$$k = k^{(0)} \left(1 - \frac{1}{2} I_c \Delta\epsilon_c\right) + O(\Delta\epsilon_c^2). \tag{11}$$

We stress again that although the solution (8) does not require smallness of $\Delta\epsilon_c$, it is still approximate since it neglects contribution of all unperturbed modes other than the BIC. In contrast the first order non-degenerate RS solution (11) only involves a single mode but requires smallness of $\Delta\epsilon$. Notice though, that Eq. (8) and Eq. (11) coincide up to $O(\Delta\epsilon_c^2)$. Thus, the Wigner-Brillouin approach truncated to a single eigenstates produces an exact result up to $O(\Delta\epsilon_c^2)$.

Unfortunately, unlike $\mathscr{L}_c$ the effect of $\mathscr{L}_\theta$ can not be described by the single state WB approach. This is because the perturbed solution is a radiating state and, thus, even in the first order approximation can not be written through the non-radiating unperturbed BIC. Physically, the application of $\mathscr{L}_\theta$ generates the dispersion of the leaky band hosting the BIC in the Γ-point. Since the band is symmetric with respect to $\beta \to -\beta$ the dispersion about the Γ-point reads

$$k = k^{(0)}(1 + \alpha\theta^2) + O(\theta^4). \tag{12}$$

The complex-valued parameter α can be found by fitting to numerical or experimental data. As it was already mentioned the corrections due to $\mathscr{L}_c$ and $\mathscr{L}_\theta$ are additive in the leading order because both θ and Δn_c are regarded as small quantities. Thus, using $\lambda = 2\pi/k$, Eq. (8), and Eq. (12) we obtain the resonant wavelength, λ_{res} as

$$\lambda_{\mathrm{res}} = \lambda_{\mathrm{BIC}}^{(0)} \left(1 + \frac{1}{2} I_c \Delta\epsilon_c - \alpha\theta^2\right). \tag{13}$$

Notice that Eq. (13) explicitly predicts blue shift of the resonant wavelength with positive $\Delta\epsilon_c$ in the first perturbation order when α is independent of $\Delta\epsilon_c$. Applying the definition of the

Optics EXPRESS

sensitivity, Eq. (2) one finds

$$S = \lambda_{\mathrm{BIC}}^{(0)} n_c^{(0)} I_c. \tag{14}$$

The above expression for sensitivity exactly coincides with that previously derived by Mortensen, Xiao, and Pedersen [40] for guided modes in a bulk photonic crystal.

Remarkably, Eq. (14) can also be derived with a straightforward application of the Hellmann-Feynman (HF) theorem [42]. Notice, though, that the HF theorem strictly requires the problem to be described by Hermitian operators. In general the radiating boundary conditions break the hermiticity. However, in the case of the BIC proper the eigenfield is localized about the DG and, thus, is not affected by the boundary condition in the far-zone.

To derive the FOM we recall that the width W of a high-Q resonance can be written as

$$W = \frac{\lambda_{\mathrm{BIC}}^{(0)}}{Q}, \tag{15}$$

where Q is the quality factor

$$Q = \frac{k^{(0)}}{2\Im\{a\}\theta^2}. \tag{16}$$

Hence, for the FOM we have

$$\mathrm{FOM} = n_c^{(0)} I_c Q \propto \theta^{-2}. \tag{17}$$

Here we would like to mention an alternative definition of the FOM as the product between the Q-factor and the sensitivity [43]. One can see from Eq. (14) and Eq. (17) that both FOMs exhibit the same dependence on θ up to a constant prefactor.

Finally, let us discuss the upper limit of the differential sensitivity. By comparing the integral (9) against Eq. (10) one writes

$$I_c = \frac{1}{\epsilon_c}\left[1 - \int_{\mathcal{S}_{\mathrm{DG}}} \epsilon(y,z)\left(E_x^{(\mathrm{BIC})}\right)^2 dydz\right], \tag{18}$$

where $\mathcal{S}_{\mathrm{DG}}$ is the area of the elementary cell occupied by the DG. The quantity I_c reaches its maximal value, when the integral in Eq. (18) equals to zero. Thus, the maximal differential sensitivity in the spectral vicinity of an isolated BIC is given by

$$S_{\max} = \frac{\lambda_{\mathrm{BIC}}}{n_c}. \tag{19}$$

4. Numerical results

To verify the above findings we run FDTD simulations for computing the transmittance, T as a function of both k and θ. In Fig. 2(a) we demonstrate the blue shift of the Fano feature with the increase of the cladding RI. In Figs. 2(b-d) we plotted the shift of the resonant wavelength $\Delta\lambda_{\mathrm{res}} = \lambda_{\mathrm{res}}^{(0)} - \lambda_{\mathrm{res}}$ in comparison against Eq. (13) at three different values of θ. On can see from Figs. 2(b-d) that the data match with deviation only becoming visible at a larger angle of incidence, $\theta = 4$, (deg), when the higher perturbation orders in θ come into play.

In Table 2 we present the numerical values of differential sensitivity obtained from Figs. 2(b-d) in comparison against the analytic result Eq. (14). To assess the accuracy of Eq. (14) we calculated the relative error

$$\delta = \frac{|S_{\mathrm{theor}} - S_{\mathrm{num}}|}{2(S_{\mathrm{theor}} + S_{\mathrm{num}})} \cdot 100\%, \tag{20}$$

where S_{theor} stands for the theoretical value of the sensitivity found from Eq. (14), while S_{num} is used for numerical data. Again one can see a good coincidence with δ>1% only for $\theta = 4$,

Optics EXPRESS

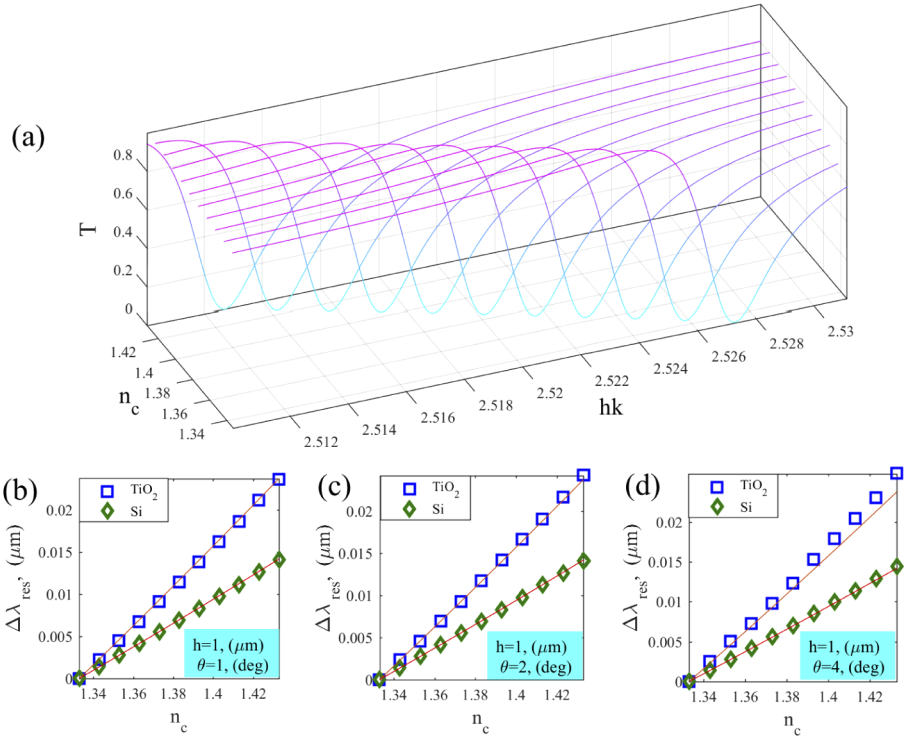

Fig. 2. Blue shift of the resonant frequency. (a) Fano feature in transmittance, T against the incident wave number, kh and the refractive index of the cladding fluid, n_c; the DG is made of Si and illuminated at the angle of incidence $\theta = 4$, (deg). (b-d) Shift of the resonant wavelength, $\Delta\lambda_{\text{res}}$ as a function of n_c at three different angles of incidence; DG material and θ are specified in the subplots.

(deg) with a TiO_2 DG. Otherwise the sensitivity remains constant about the normal incidence as predicted by Eq. (14).

In Fig. 3(a) we show the Fano feature in transmittance collapsing on approach to normal incidence. The width of the resonances is extracted from the data in Fig. 3(a) and plotted against θ^2 in Fig. 3(b). One can see from Fig. 3(b) that the numerical data comply with Eq. (15) and Eq. (16) which predict $W \propto \theta^2$. Finally, in Fig. 3(c) we plot the FOM against the angle of incidence together with fitting curves FOM $\propto \theta^{-2}$. One can see that the numerical results are in accordance to Eq. (17).

Table 2. Numerical and theoretical values of sensitivity. RIU stands for refractive index unit.

Grating material	Si	Si	Si	TiO_2	TiO_2	TiO_2
θ, (deg)	1	2	4	1	2	4
S_{theor}, (nm/RIU)	137.2	137.2	137.2	229.7	229.7	229.7
S_{num}, (nm/RIU)	137.4	137.5	137.8	222.4	233.7	252.3
δ	0.037%	0.052%	0.114%	0.812%	0.429%	2.343%

Optics EXPRESS

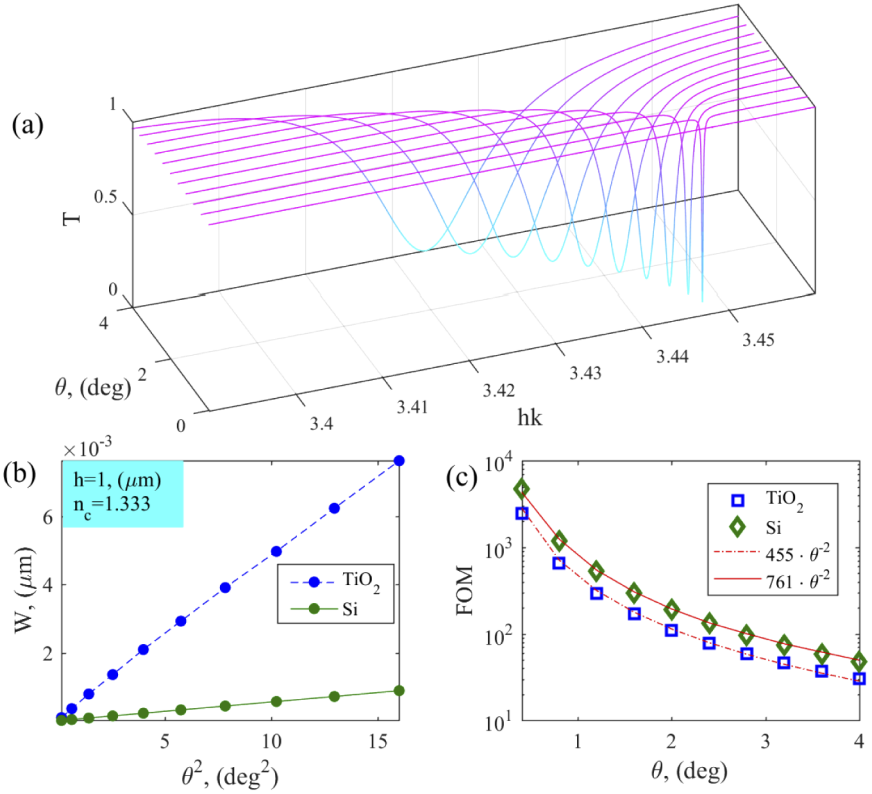

Fig. 3. Fano resonance and FOM. (a) Collapsing Fano feature in transmittance, T on approach to the normal incidence in TiO_2 DG; $n_c = 1.333$. (b) Resonant width in terms of wavelength against θ^2. (c) FOM as a function of the angle of incidence. Thin lines show fitting to FOM $\propto \theta^{-2}$.

5. Summary and conclusions

The equations derived provide a cue to designing an efficient sensor with an optical BIC. The expression for sensitivity obtained in this paper is identical to that derived by Mortensen, Xiao, and Pedersen [40] for bulk photonic crystal underlying the unique properties of BICs among the leaky modes supported by the grating. In this paper we limited ourselves with in-Γ symmetry protected TE BICs. We mention in passing that the theory can be directly applied to TM polarization [44] or non-symmetry protected (accidental) off-Γ BICs [14,45–47]. In the latter case, the sensor would be operating at oblique incidence. The only theoretical difference is that the dispersion of the real part of the resonant frequency would be linear in the vicinity of the BIC point. This, however, would not modify the final expression for the sensitivity Eq. (14). At the same time, the dispersion of the imaginary part is still parabolic because the radiation loss rates are non-negative. Thus, FOM $\propto (\theta - \theta_{\mathrm{BIC}})^{-2}$, where θ_{BIC} is the incidence angle corresponding to the off-Γ BIC.

According to Eq. (14), and Eq. (18) the obvious approach for maximising the sensitivity is either manufacturing the DG of a dielectric with small ϵ or choosing a BIC with the eigenfield predominantly occupying the free space above the DG. Both design paradigms can be implemented by solving the eignevalue problem with FDTD method with variation of the geometric parameters.

On the other hand, the FOM can be optimized by operating at near normal incidence. At this point some comments are due in regard to FOM, Eq. (17) diverging with the decrease of the

Optics EXPRESS

angle of incidence. Experimentally, a zero linewidth cannot be obtained in a realistic set-up due to three major factors:

(i) material losses due to absorption in the dielectric [48,49];

(ii) fabrication inaccuracies [50]; and

(iii) finiteness of the structure [48,51], as the BIC proper cannot be supported by systems finite in all spatial dimensions [52].

The effect of all three factors is saturation of FOM on approach to normal incidence. Which of the three will dominate in the saturation is determined by a specific design of the DG.

Another important aspect is the finite waist of the Gaussian beam illuminating the DG. Equations (14), and (17) can only be strictly applied to a plane wave, whereas a Gaussian beam is always a continuum of plane waves propagating to slightly different directions. Miniaturization of the sensor would imply a tightly focused beam with a broad momentum distribution in the Fourier plane. This would naturally compromise the FOM, as the scattering channels with larger angles of incidence become more populated.

Finally, let us discuss whether the limit, Eq. (19) can be overcome. First of all, Eq. (19) is derived under assumption of smallness of the perturbation operators. Therefore, the sensitivities larger than Eq. (19) are not strictly forbidden. For example, a larger sensitivity has been recently reported with surface plasmon-polaritons [53]. The drawback, however, is the drop of the quality factor due to strong coupling of the eigenmode to the outgoing waves. Thus, the increase of sensitivity with departure from the BIC proper can be only obtained at the cost of the sensor FOM. More promising is optimizing the sensitivity while keeping the high FOM intact. This can be done by breaking the second condition in derivation of Eq. (19), namely, the single mode approach. One possible route is looking for a BIC in the exceptional points [54–56], which unavoidably emerge as a result of an intricate interplay between two eigenmodes. The other possible route is application of BIC existing just below the first Wood's anomaly in which case the contribution of the evanescent channels corresponding to the first diffraction order becomes extremely sensitive to the system's parameters [17]. The destruction of a BIC in crossing the Wood's anomaly inherently implies application of a multimodal perturbative approach since the contribution of states with finite live-time is required. We speculate that operating in the vicinity of the Wood's anomaly may result in a significant gain in sensitivity while keeping diverging the FOM and quality factor.

Funding

Ministry of Science and Higher Education of the Russian Federation (FSRZ-2020-008).

Acknowledgments

The research was supported by the Ministry of Science and High Education of Russian Federation, project no. FSRZ-2020-008. DNM is grateful to Andrey A. Bogdanov for useful discussion.

Disclosures

The authors declare that there are no conflicts of interest related to this article.

References

1. M. I. Molina, A. E. Miroshnichenko, and Y. S. Kivshar, "Surface bound states in the continuum," Phys. Rev. Lett. **108**(7), 070401 (2012).
2. S. Romano, G. Zito, S. Managò, G. Calafiore, E. Penzo, S. Cabrini, A. C. D. Luca, and V. Mocella, "Surface-enhanced raman and fluorescence spectroscopy with an all-dielectric metasurface," J. Phys. Chem. C **122**(34), 19738–19745 (2018).
3. E. N. Bulgakov and A. F. Sadreev, "Bound states in the continuum in photonic waveguides inspired by defects," Phys. Rev. B **78**(7), 075105 (2008).

Optics EXPRESS

4. R. Porter and D. Evans, "Embedded Rayleigh-bloch surface waves along periodic rectangular arrays," Wave Motion **43**(1), 29–50 (2005).
5. E. Penzo, S. Romano, Y. Wang, S. Dhuey, L. Dal Negro, V. Mocella, and S. Cabrini, "Patterning of electrically tunable light-emitting photonic structures demonstrating bound states in the continuum," J. Vac. Sci. Technol., B: Nanotechnol. Microelectron.: Mater., Process., Meas., Phenom. **35**(6), 06G401 (2017).
6. B. Zhen, C. W. Hsu, L. Lu, A. D. Stone, and M. Soljačić, "Topological nature of optical bound states in the continuum," Phys. Rev. Lett. **113**(25), 257401 (2014).
7. V. Mocella and S. Romano, "Giant field enhancement in photonic resonant lattices," Phys. Rev. B **92**(15), 155117 (2015).
8. K. Koshelev, A. Bogdanov, and Y. Kivshar, "Meta-optics and bound states in the continuum," Sci. Bull. **64**(12), 836–842 (2019).
9. K. Koshelev, G. Favraud, A. Bogdanov, Y. Kivshar, and A. Fratalocchi, "Nonradiating photonics with resonant dielectric nanostructures," Nanophotonics **8**(5), 725–745 (2019).
10. G. Zito, S. Romano, S. Cabrini, G. Calafiore, A. C. De Luca, E. Penzo, and V. Mocella, "Observation of spin-polarized directive coupling of light at bound states in the continuum," Optica **6**(10), 1305–1312 (2019).
11. L. Yuan and Y. Y. Lu, "Strong resonances on periodic arrays of cylinders and optical bistability with weak incident waves," Phys. Rev. A **95**(2), 023834 (2017).
12. S. P. Shipman and S. Venakides, "Resonant transmission near nonrobust periodic slab modes," Phys. Rev. E **71**(2), 026611 (2005).
13. A. F. Sadreev, E. N. Bulgakov, and I. Rotter, "Bound states in the continuum in open quantum billiards with a variable shape," Phys. Rev. B **73**(23), 235342 (2006).
14. C. Blanchard, J.-P. Hugonin, and C. Sauvan, "Fano resonances in photonic crystal slabs near optical bound states in the continuum," Phys. Rev. B **94**(15), 155303 (2016).
15. E. N. Bulgakov and D. N. Maksimov, "Optical response induced by bound states in the continuum in arrays of dielectric spheres," J. Opt. Soc. Am. B **35**(10), 2443 (2018).
16. S. Romano, G. Zito, S. Torino, G. Calafiore, E. Penzo, G. Coppola, S. Cabrini, I. Rendina, and V. Mocella, "Label-free sensing of ultralow-weight molecules with all-dielectric metasurfaces supporting bound states in the continuum," Photonics Res. **6**(7), 726 (2018).
17. S. Romano, G. Zito, S. N. L. Yépez, S. Cabrini, E. Penzo, G. Coppola, I. Rendina, and V. Mocellaa, "Tuning the exponential sensitivity of a bound-state-in-continuum optical sensor," Opt. Express **27**(13), 18776 (2019).
18. M. E. Beheiry, V. Liu, S. Fan, and O. Levi, "Sensitivity enhancement in photonic crystal slab biosensors," Opt. Express **18**(22), 22702 (2010).
19. Y. Liu, W. Zhou, and Y. Sun, "Optical refractive index sensing based on high-Q bound states in the continuum in free-space coupled photonic crystal slabs," Sensors **17**(8), 1861 (2017).
20. S. Romano, A. Lamberti, M. Masullo, E. Penzo, S. Cabrini, I. Rendina, and V. Mocella, "Optical biosensors based on photonic crystals supporting bound states in the continuum," Materials **11**(4), 526 (2018).
21. F. Yesilkoy, E. R. Arvelo, Y. Jahani, M. Liu, A. Tittl, V. Cevher, Y. Kivshar, and H. Altug, "Ultrasensitive hyperspectral imaging and biodetection enabled by dielectric metasurfaces," Nat. Photonics **13**(6), 390–396 (2019).
22. S. Mukherjee, J. Gomis-Bresco, P. Pujol-Closa, D. Artigas, and L. Torner, "Angular control of anisotropy-induced bound states in the continuum," Opt. Lett. **44**(21), 5362 (2019).
23. H. Vyas and R. S. Hegde, "Improved refractive-index sensing performance in medium contrast gratings by asymmetry engineering," Opt. Mater. Express **10**(7), 1616 (2020).
24. N. Bosio, H. Šípová-Jungová, N. O. Länk, T. J. Antosiewicz, R. Verre, and M. Käll, "Plasmonic versus all-dielectric nanoantennas for refractometric sensing: A direct comparison," ACS Photonics **6**(6), 1556–1564 (2019).
25. D. C. Marinica, A. G. Borisov, and S. V. Shabanov, "Bound states in the continuum in photonics," Phys. Rev. Lett. **100**(18), 183902 (2008).
26. F. Monticone and A. Alù, "Bound states within the radiation continuum in diffraction gratings and the role of leaky modes," New J. Phys. **19**(9), 093011 (2017).
27. E. N. Bulgakov, D. N. Maksimov, P. N. Semina, and S. A. Skorobogatov, "Propagating bound states in the continuum in dielectric gratings," J. Opt. Soc. Am. B **35**(6), 1218–1222 (2018).
28. E. N. Bulgakov and D. N. Maksimov, "Avoided crossings and bound states in the continuum in low-contrast dielectric gratings," Phys. Rev. A **98**(5), 053840 (2018).
29. S.-G. Lee and R. Magnusson, "Band dynamics of leaky-mode photonic lattices," Opt. Express **27**(13), 18180 (2019).
30. D. A. Bykov, E. A. Bezus, and L. L. Doskolovich, "Coupled-wave formalism for bound states in the continuum in guided-mode resonant gratings," Phys. Rev. A **99**(6), 063805 (2019).
31. X. Gao, B. Zhen, M. Soljačić, H. Chen, and C. W. Hsu, "Bound states in the continuum in fiber bragg gratings," ACS Photonics **6**(11), 2996–3002 (2019).
32. Z. F. Sadrieva, I. S. Sinev, K. L. Koshelev, A. Samusev, I. V. Iorsh, O. Takayama, R. Malureanu, A. A. Bogdanov, and A. V. Lavrinenko, "Transition from optical bound states in the continuum to leaky resonances: Role of substrate and roughness," ACS Photonics **4**(4), 723–727 (2017).
33. H. Hemmati and R. Magnusson, "Resonant dual-grating metamembranes supporting spectrally narrow bound states in the continuum," Adv. Opt. Mater. **7**(20), 1900754 (2019).
34. Y. B. Zel'dovich, "On the theory of unstable states," Sov. Phys. JETP **12**, 542–548 (1961).

Optics EXPRESS

35. H. M. Lai, P. T. Leung, K. Young, P. W. Barber, and S. C. Hill, "Time-independent perturbation for leaking electromagnetic modes in open systems with application to resonances in microdroplets," Phys. Rev. A **41**(9), 5187–5198 (1990).
36. P. Lalanne, W. Yan, K. Vynck, C. Sauvan, and J.-P. Hugonin, "Light interaction with photonic and plasmonic resonances," Laser Photonics Rev. **12**(5), 1700113 (2018).
37. E. A. Muljarov, W. Langbein, and R. Zimmermann, "Brillouin-Wigner perturbation theory in open electromagnetic systems," Europhys. Lett. **92**(5), 50010 (2010).
38. S. V. Lobanov, W. Langbein, and E. A. Muljarov, "Resonant-state expansion of three-dimensional open optical systems: Light scattering," Phys. Rev. A **98**(3), 033820 (2018).
39. P. S. Pankin, D. N. Maksimov, K.-P. Chen, and I. V. Timofeev, "Fano feature induced by a bound state in the continuum via resonant state expansion," Sci. Rep. **10**(1), 13691 (2020).
40. N. A. Mortensen, S. Xiao, and J. Pedersen, "Liquid-infiltrated photonic crystals: enhanced light-matter interactions for lab-on-a-chip applications," Microfluid. Nanofluid. **4**(1-2), 117–127 (2008).
41. L. D. Landau and E. M. Lifshitz, Quantum Mechanics: Non-relativistic Theory. V. 3 of Course of Theoretical Physics (Pergamon Press, 1958).
42. P. Politzer and J. S. Murray, "The Hellmann-Feynman theorem: a perspective," J. Mol. Model. **24**(9), 266 (2018).
43. G. Pitruzzello and T. F. Krauss, "Photonic crystal resonances for sensing and imaging," J. Opt. **20**(7), 073004 (2018).
44. Z. Hu and Y. Y. Lu, "Standing waves on two-dimensional periodic dielectric waveguides," J. Opt. **17**(6), 065601 (2015).
45. C. W. Hsu, B. Zhen, J. Lee, S.-L. Chua, S. G. Johnson, J. D. Joannopoulos, and M. Soljačić, "Observation of trapped light within the radiation continuum," Nature **499**(7457), 188–191 (2013).
46. A. Taghizadeh and I.-S. Chung, "Quasi bound states in the continuum with few unit cells of photonic crystal slab," Appl. Phys. Lett. **111**(3), 031114 (2017).
47. L. Ni, Z. Wang, C. Peng, and Z. Li, "Tunable optical bound states in the continuum beyond in-plane symmetry protection," Phys. Rev. B **94**(24), 245148 (2016).
48. Z. F. Sadrieva, M. A. Belyakov, M. A. Balezin, P. V. Kapitanova, E. A. Nenasheva, A. F. Sadreev, and A. A. Bogdanov, "Experimental observation of a symmetry-protected bound state in the continuum in a chain of dielectric disks," Phys. Rev. A **99**(5), 053804 (2019).
49. Z. Hu, L. Yuan, and Y. Y. Lu, "Bound states with complex frequencies near the continuum on lossy periodic structures," Phys. Rev. A **101**(1), 013806 (2020).
50. L. Ni, J. Jin, C. Peng, and Z. Li, "Analytical and statistical investigation on structural fluctuations induced radiation in photonic crystal slabs," Opt. Express **25**(5), 5580 (2017).
51. E. N. Bulgakov and D. N. Maksimov, "Light enhancement by quasi-bound states in the continuum in dielectric arrays," Opt. Express **25**(13), 14134 (2017).
52. M. G. Silveirinha, "Trapping light in open plasmonic nanostructures," Phys. Rev. A **89**(2), 023813 (2014).
53. R. G. Bikbaev, S. Y. Vetrov, and I. V. Timofeev, "Hybrid Tamm and surface plasmon polaritons in resonant photonic structure," J. Quant. Spectrosc. Radiat. Transfer **253**, 107156 (2020).
54. R. El-Ganainy, M. Khajavikhan, D. N. Christodoulides, and S. K. Ozdemir, "The dawn of non-Hermitian optics," Commun. Phys. **2**(1), 37 (2019).
55. š. K. özdemir, S. Rotter, F. Nori, and L. Yang, "Parity–time symmetry and exceptional points in photonics," Nat. Mater. **18**(8), 783–798 (2019).
56. A. Krasnok, D. Baranov, H. Li, M.-A. Miri, F. Monticone, and A. Alú, "Anomalies in light scattering," Adv. Opt. Photonics **11**(4), 892 (2019).